J|A|C|S ARTICLES

Published on Web 06/24/2010

Magnetic Conjugated Polymer Nanoparticles as Bimodal Imaging Agents

Philip Howes,[†] Mark Green,*[,†] Alex Bowers,[†] David Parker,[†] Gopal Varma,[§] Mathew Kallumadil,[⊥] Mary Hughes,[‡] Alice Warley,[||] Anthony Brain,[||] and Rene Botnar[§]

Department of Physics, King's College London, Strand, London WC2R 2LS, U.K., School of Biomedical and Health Sciences, Waterloo Campus, King's College London, Franklin-Wilkins Building, Stamford Street, London SE1 9NH, U.K., Division of Imaging Sciences, King's College London, St. Thomas' Hospital, London SE1 7EH, U.K., Centre for Ultrastructural Imaging, King's College London, New Hunt's House, Guy's Campus, London SE1 1UL, U.K., and London Centre for Nanotechnology, University College London, 17-19 Gordon Street, London WC1 H 0AH, U.K.

Received April 14, 2010; E-mail: mark.a.green@kcl.ac.uk

Abstract: Hybrid nanoparticles which incorporate multiple functionalities, such as fluorescence and magnetism, can exhibit enhanced efficiency and versatility by performing several tasks in parallel. In this study, magnetic-fluorescent semiconductor polymer nanospheres (MF-SPNs) have been synthesized by encapsulation of hydrophobic conjugated polymers and iron oxide nanoparticles in phospholipid micelles. Four fluorescent conjugated polymers were used, yielding aqueous dispersions of nanoparticles which emit across the visible spectrum. The MF-SPNs were shown to be magnetically responsive and simultaneously fluorescent. In MRI studies, they were seen to have a shortening effect on the transverse T_2* relaxation time, which demonstrates their potential as an MR contrast agent. Finally, successful uptake of the MF-SPNs by SH-SY5Y neuroblastoma cells was demonstrated, and they were seen to behave as bright and stable fluorescent markers. There was no evidence of toxicity or adverse affect on cell growth.

Introduction

The possibility of bringing together several different functional materials into a single nanostructure offers great potential for increased efficiency and versatility in the numerous applications of nanomaterials in practical science. These hybrid nanostructures combine the specific functionality of their constituent parts in a multifunctional tool which can perform several tasks in parallel.[1] Fluorescent-magnetic hybrid nanoparticles have been of particular interest in the development of diagnostic and therapeutic materials.[2] By combining these two functionalities it is hoped that robust fluorescent nanoparticles are created which can be physically manipulated by an external magnetic field or provide contrast enhancement in magnetic resonance imaging (MRI).[3,4] With the addition of functionalized surfactants, it is easy to envisage a wealth of applications evolving for these multimodal nanoparticles.

Fluorescent-magnetic nanoparticles offer new opportunities for *in vivo* applications in biology. By functionalizing these nanoparticles with targeting ligands (such as biomolecules[5]) it will be possible to target specific structures and tissues *in vivo*. A particularly exciting application of fluorescent-magnetic nanoparticles in this instance would be to target specific areas, such as a tumor, to localize the nanoparticles in the region of interest. Consequently, the magnetic modality would facilitate the use of MRI for preoperative localization of the targeted structure, and the fluorescence modality would be used as an intraoperative guide to provide accurate delineation between the targeted and surrounding tissues.[1,6] This has been demonstrated by the imaging of brain tumors and sentinel lymph nodes in rats.[6,7] Furthermore, it is hoped that localized delivery of fluorescent-magnetic nanoparticles could also be achieved by manipulation with an external magnetic field.[8] There are also potential applications in nanomedicine, which would combine diagnostic and therapeutic functions as nanoparticle surfaces can be functionalized with active bioagents (drugs, proteins, etc).[9,10] Other examples of *in vivo* applications include cell tracking and sorting.[11]

[†] Department of Physics, King's College London.
[‡] School of Biomedical and Health Sciences, King's College London.
[§] Division of Imaging Sciences, King's College London.
[||] Centre for Ultrastructural Imaging, King's College London.
[⊥] Centre for Nanotechnology, University College London.

(1) Quarta, A.; Di Corato, R.; Manna, L.; Ragusa, A.; Pellegrino, T. *IEEE Trans. Nanobioscience* **2007**, *6*, 298–308.
(2) Mulder, W. J. M.; Griffioen, A. W.; Strijkers, G. J.; Cormode, D. P.; Nicolay, K.; Fayad, Z. A. *Nanomedicine* **2007**, *2*, 307–324.
(3) Waters, E. A.; Wickline, S. A. *Basic Res. Cardiol.* **2008**, *103*, 114–121.
(4) Gao, J. H.; Zhang, W.; Huang, P. B.; Zhang, B.; Zhang, X. X.; Xu, B. *J. Am. Chem. Soc.* **2008**, *130*, 3710–3711.
(5) De, M.; Ghosh, P. S.; Rotello, V. M. *Adv. Mater.* **2008**, *20*, 4225–4241.
(6) Kircher, M. F.; Mahmood, U.; King, R. S.; Weissleder, R.; Josephson, L. *Cancer Res.* **2003**, *63*, 8122–8125.
(7) Josephson, L.; Kircher, M. F.; Mahmood, U.; Tang, Y.; Weissleder, R. *Bioconjugate Chem.* **2002**, *13*, 554–560.
(8) Majewski, P.; Thierry, B. *Crit. Rev. Solid State Mater. Sci.* **2007**, *32*, 203–215.

The development of fluorescent-magnetic nanocomposites is at a relatively early stage. However, several approaches have been taken with some interesting results.[12] One approach is to have a magnetic core which is encapsulated in a fluorescent shell. For example, CdS shells have been grown on FePt cores[13] and organic fluorophores have been deposited on silica capped magnetic cores.[14,15] Another approach is to coat a fluorescent nanoparticle with a magnetic capping layer. This has been achieved by synthesizing CdS:Mn/ZnS quantum dots in a water-in-oil microemulsion, creating a fluorescent and paramagnetic nanostructure.[16] Although quantum dots provide a bright, stable, and versatile fluorescent functionality to bifunctional nanomaterials, they are inherently toxic as most contain materials such as cadmium. Thus toxicity will always remain a concern for their use in biological applications.[17−22] Other fluorescent materials have been used in fluorescent-magnetic nanoparticles. For example, fluorescent dyes such as fluorescein isothiocyanate (FITC)[23] and Cy5.5[6] have been combined with iron oxide. However, dyes such as these have inherent problems with photobleaching and wide emission lines.[24]

Conjugated polymers have emerged as a promising class of functional material in the production of fluorescent nanoparticles. These organic polymers exhibit semiconductor characteristics due to their conjugated backbone structure, where alternating single and double bonds give rise to π-electron delocalization and a band structure, akin to classical inorganic semiconductors. Historically, a large amount of conjugated polymer research has been directed toward producing electronic devices, such as LEDs and photovoltaics, due to their excellent photo- and electroluminescent properties.[25,26] However, recently they have gained attention as materials for fluorescent nanoparticle production, which are commonly referred to as semiconducting polymer nanospheres (SPNs). This is because they not only exhibit bright and stable emission, with high extinction coefficients and quantum yields in solution,[27] but also are biologically compatible[28] and should overcome the cytotoxicity problems associated with quantum dots.[17,18,29,30] Importantly, as they are polymeric, they combine the ease of processing and mechanical properties of plastics with the optoelectronic properties of semiconductors.[25]

SPNs have been used in various cell imaging studies, where they have been seen to function as bright and stable fluorescent markers.[31−33] Importantly, no evidence of cellular toxicity has been observed. SPNs exhibit versatile optical properties as their characteristics can be tuned by changing the constituent polymer,[33,34] creating polymer blends,[35] and by doping them with other dyes.[36] One of the most common methods of synthesis of SPNs is the reprecipitation method, which sees conjugated polymers precipitate as small (usually sub-20 nm) particles due to conflicting solvent interactions and rapid mixing.[27,33,37] Another method of synthesis is by miniemulsion, which employs a highly sheared heterophase system to create dispersions of polymer nanoparticles.[38,39] Although this method gives particles with surfactants, such as sodium dodecyl sulfate (SDS)[38] or poly(ethylene glycol) (PEG),[31,32] the size of the particles has tended to be large or the size distributions are hard to control.

Recently, we have developed a new method of synthesis of SPNs by encapsulating them in PEG-phospholipids.[40] This method differs from the others as it does not rely on mechanical agitation of the system; rather formation is driven by the formation of micelles from the amphiphilic phospholipid molecules. The result is that nanoparticles will form in very mild reaction conditions. These SPNs were shown to exhibit high colloidal stability, they were effectively taken up by cells in imaging experiments where they showed no signs of toxicity, and they were successfully conjugated to proteins.

PEG conjugated phospholipids were employed in the above work. Phospholipids are commonly used in biomedical applications where, for example, they have been used to control circulation and release of drugs *in vivo*. PEG is used to increase the circulation lifetime of materials *in vivo* as it decreases detection and clearance from the body by the reticuloendothelial system,[41] and the incorporation of PEG-phospholipids into the liposomal structures has been shown to increase circulation time

(9) Byrne, J. D.; Betancourt, T.; Brannon-Peppas, L. *Adv. Drug Delivery Rev.* **2008**, *60*, 1615–1626.
(10) Meziani, M. J.; Pathak, P.; Harruff, B. A.; Hurezeanu, R.; Sun, Y. P. *Langmuir* **2005**, *21*, 2008–2011.
(11) Lu, C.-W.; Hung, Y.; Hsiao, J.-K.; Yao, M.; Chung, T.-H.; Lin, Y.-S.; Wu, S.-H.; Hsu, S.-C.; Liu, H.-M.; Mou, C.-Y.; Yang, C.-S.; Huang, D.-M.; Chen, Y.-C. *Nano Lett.* **2006**, *7*, 149–154.
(12) Corr, S. A.; Rakovich, Y. P.; Gun'ko, Y. K. *Nanoscale Res. Lett.* **2008**, *3*, 87–104.
(13) Gu, H.; Zheng, R.; Zhang, X.; Xu, B. *J. Am. Chem. Soc.* **2004**, *126*, 5664–5665.
(14) Lu, Y.; Yin, Y.; Mayers, B. T.; Xia, Y. *Nano Lett.* **2002**, *2*, 183–186.
(15) Lin, Y.-S.; Wu, S.-H.; Hung, Y.; Chou, Y.-H.; Chang, C.; Lin, M.-L.; Tsai, C.-P.; Mou, C.-Y. *Chem. Mater.* **2006**, *18*, 5170–5172.
(16) Santra, S.; Yang, H.; Holloway, P. H.; Stanley, J. T.; Mericle, R. A. *J. Am. Chem. Soc.* **2005**, *127*, 1656–1657.
(17) Derfus, A. M.; Chan, W. C. W.; Bhatia, S. N. *Nano Lett.* **2004**, *4*, 11–18.
(18) Hoshino, A.; Fujioka, K.; Oku, T.; Suga, M.; Sasaki, Y. F.; Ohta, T.; Yasuhara, M.; Suzuki, K.; Yamamoto, K. *Nano Lett.* **2004**, *4*, 2163–2169.
(19) Kirchner, C.; Liedl, T.; Kudera, S.; Pellegrino, T.; Javier, A. M.; Gaub, H. E.; Stolzle, S.; Fertig, N.; Parak, W. J. *Nano Lett.* **2005**, *5*, 331–338.
(20) Cai, W. B.; Hsu, A. R.; Li, Z. B.; Chen, X. Y. *Nanoscale Res. Lett.* **2007**, *2*, 265–281.
(21) Delehanty, J. B.; Mattoussi, H.; Medintz, I. L. *Anal. Bioanal. Chem.* **2009**, *393*, 1091–1105.
(22) Aillon, K. L.; Xie, Y. M.; El-Gendy, N.; Berkland, C. J.; Forrest, M. L. *Adv. Drug Delivery Rev.* **2009**, *61*, 457–466.
(23) Bertorelle, F.; Wilhelm, C.; Roger, J.; Gazeau, F.; Menager, C.; Cabuil, V. *Langmuir* **2006**, *22*, 5385–5391.
(24) Parak, W. J.; Pellegrino, T.; Plank, C. *Nanotechnology* **2005**, *16*, R9–R25.
(25) Schwartz, B. J. *Annu. Rev. Phys. Chem.* **2003**, *54*, 141–172.
(26) Dini, D. *Chem. Mater.* **2005**, *17*, 1933–1945.
(27) Wu, C. F.; Szymanski, C.; McNeill, J. *Langmuir* **2006**, *22*, 2956–2960.
(28) Guimard, N. K.; Gomez, N.; Schmidt, C. E. *Prog. Polym. Sci.* **2007**, *32*, 876–921.
(29) Liang, J. G.; He, Z. K.; Zhang, S. S.; Huang, S.; Ai, X. P.; Yang, H. X.; Han, H. Y. *Talanta* **2007**, *71*, 1675–1678.
(30) Anas, A.; Akita, H.; Harashima, H.; Itoh, T.; Ishikawa, M.; Biju, V. *J. Phys. Chem. B* **2008**, *112*, 10005–10011.
(31) Green, M.; Howes, P.; Berry, C.; Argyros, O.; Thanou, M. *Proc. R. Soc. London, Ser. A* **2009**, *465*, 2751–2759.
(32) Howes, P.; Thorogate, R.; Green, M.; Jickells, S.; Daniel, B. *Chem. Commun.* **2009**, 2490–2492.
(33) Wu, C.; Bull, B.; Szymanski, C.; Christensen, K.; McNeill, J. *ACS Nano* **2008**, *2*, 2415–2423.
(34) Li, K.; Pan, J.; Feng, S. S.; Wu, A. W.; Pu, K. Y.; Liu, Y. T.; Liu, B. *Adv. Funct. Mater.* **2009**, *19*, 3535–3542.
(35) Wu, C.; Peng, H.; Jiang, Y.; McNeill, J. *J. Phys. Chem. B* **2006**, *110*, 14148–14154.
(36) Wu, C. F.; Zheng, Y. L.; Szymanski, C.; McNeill, J. *J. Phys. Chem. C* **2008**, *112*, 1772–1781.
(37) Wu, C. F.; Szymanski, C.; Cain, Z.; McNeill, J. *J. Am. Chem. Soc.* **2007**, *129*, 12904–12905.
(38) Landfester, K.; Montenegro, R.; Scherf, U.; Guntner, R.; Asawapirom, U.; Patil, S.; Neher, D.; Kietzke, T. *Adv. Mater.* **2002**, *14*, 651–655.
(39) Landfester, K. *Annu. Rev. Mater. Res.* **2006**, *36*, 231–279.
(40) Howes, P.; Green, M.; Levitt, J.; Suhling, K.; Hughes, M. *J. Am. Chem. Soc.* **2010**, *132*, 3989–3996.

while maintaining the targeting ability of drug-loaded liposomes.[42,43] In other areas of nanoparticle research, phospholipids and PEG-phospholipids are commonly used as phase transfer agents and as a means of increasing the biocompatibility of nanoparticles, such as quantum dots.[44−46]

In an extension to our previous work on conjugated polymer micelles, we have incorporated superparamagnetic iron oxide nanoparticles (SPIONs) into the SPN structure to create magnetic-fluorescent semiconducting polymer nanospheres (MF-SPNs). Iron oxide has been widely used in magnetic resonance (MR) studies and applications.[47] Superparamagnetism arises when iron oxide nanoparticles are small enough to be a single crystal domain. These particles have no intrinsic magnetic moment, but when they are placed in an external magnetic field a local field is induced. This is important, as it means that the particles are not magnetically attracted to one another in solution and therefore stay dispersed, but they exhibit magnetic behavior when an external field is applied. Iron oxide nanoparticles are used as contrast agents in MRI as rapid signal loss is observed in areas where they are present. Additionally, the contrast induced by superparamagnetic materials is much stronger than that produced by paramagnetic materials.[48] Imaging of SPIONs *in situ* can allow visualization of structures or can be used to track the migration of materials when combined with targeting molecules.[49−51] Contrast in MR images is provided by differing phases of nuclear spins (usually hydrogen atoms) across different tissues in the body. Alignment of these nuclear spins is achieved using a powerful magnetic field, and then radio frequency electromagnet radiation is used to manipulate them and induce differing phases across the tissues. The different tissues will then produce differing signals, which can be detected and used to construct an image of the internal structures. Iron oxide contrast agents have a significant effect on the T_2 signal decay, which is based on the lifetime of the signal in the transverse plane. The T_2 signal decays a lot more rapidly in iron oxide than in normal tissue, and this strong differential in signal provides good image contrast. In the current work, MRI imaging studies where performed on MF-SPN solutions to demonstrate their MR activity and to prove their effectiveness as potential image contrast agents.

As a further demonstration of the potential for MF-SPNs to be used in biological applications, cell imaging studies were performed using MF-SPNs as fluorescent markers. To be useful biological tools, nanoparticles must be efficiently taken up by cells, have stable fluorescence, and be nontoxic. Macromolecules can be taken up by endocytosis, which is universal to all cells, or by phagocytosis, which occurs in specific cell types and is a specialized form of endocytosis. Although proposed applications of fluorescent-magnetic nanomaterials tend to be for *in vivo* applications, it is important to demonstrate they are nondestructive and functional probes *in vitro*, in cellular studies.[11,15,23,52] To assess whether nanoparticles have been taken up by cells and assess their fluorescence intracellularly it is necessary to use confocal microscopy. This technique has the resolution to allow images from the cross section of the cell from increasing depths of field to be acquired and differentiate between cell surface and intracellular fluorescence.

In this paper, a high yield synthesis of MF-SPNs, and their use in MR and cell imaging, is presented. These nanoparticles were formed by encapsulation of hydrophobic conjugated polymer chains and SPIONs in phospholipid micelles by solvent evaporation. Phosphatidycholine is often used in conjunction with PEG-phospholipids to control the density of packing of the PEG chains on the particle surface, and we have used a similar system with reference to work performed on quantum dot encapsulation.[44]

Materials and Methods

Four conjugated polymers were used in this work. Poly(2,5-di(3′,7′-dimethyloctyl)phenylene-1,4-ethynylene) (PPE, MW unknown), poly((9,9-dioctyl-2,7-divinylene-fluorenylene)-*alt*-*co*-(2-methoxy-5-(2-ethyl-hexyloxy)-1,4-phenylene)) (PFPV, MW 111 000, American Dye Source), poly((9,9-di-*n*-octylfluorenyl-2,7-diyl)-*alt*-(benzo(2,1,3)thiadiazol-4,8-diyl)) (F8BT, MW 5−8000) and poly(2-methoxy-5-(2-ethylhexyloxy)-1,4-phenylenevinylene) (MEH-PPV, MW 40−70 000). All polymers were dissolved in dichloromethane (DCM) prior to use. Oleic acid capped iron oxide nanoparticles in heptane (BioChemika 07318, 6.5 nm ± 3.0 nm) were used. All chemicals were obtained from Sigma-Aldrich unless otherwise stated. 1,2-Diacyl-*sn*-glycero-3-phosphoethanolamine-*N*-(methoxy-(polyethylene glycol)-2000) (PEG_{2000}-PE) and 1,2-dipalmitoyl-*sn*-glycero-3-phosphocholine (DPPC) were purchased from Avanti Lipids. All chemicals were used as received.

In a typical synthesis, 0.85 mg of conjugated polymer was added to 16 mL of DCM to obtain a 40 ppm solution, which was stirred for 2 days to ensure complete dissolution of the polymer. 0.5 mL (equivalent to 2.7 mg of iron oxide) of SPIONs in heptane was added to a sample vial, and the heptane was removed by isolating the solid with a magnet and decanting the solvent. The polymer solution was then added to the vial and stirred vigorously for 10 min. 7 mg of PEG_{2000}-PE and 3 mg of DPPC were added, and the solution was stirred for a further 10 min. This solution was then added to 30 mL of water under ultrasound and stirred vigorously for 20 min. After evaporation of the DCM a colored translucent solution remained. The product was filtered through filter paper and then centrifuged to remove larger particles. Magnetic nanoparticles were separated from the solution using a magnet, and the supernatant was decanted. The product was washed several times with water to remove all nonmagnetic nanoparticles. To provide a control sample for the MR studies, nonmagnetic MEH-PPV SPNs were prepared as above but without the addition of the iron oxide nanoparticles.

(41) Caliceti, P.; Veronese, F. M. *Adv. Drug Delivery Rev.* **2003**, *55*, 1261–1277.
(42) Adlakha-Hutcheon, G.; Bally, M. B.; Shew, C. R.; Madden, T. D. *Nat. Biotechnol.* **1999**, *17*, 775–779.
(43) Working, P. K.; Newman, M. S.; Sullivan, T.; Yarrington, J. *J. Pharmacol. Exp. Ther.* **1999**, *289*, 1128–1133.
(44) Dubertret, B.; Skourides, P.; Norris, D. J.; Noireaux, V.; Brivanlou, A. H.; Libchaber, A. *Science* **2002**, *298*, 1759–1762.
(45) Depalo, N.; Mallardi, A.; Comparelli, R.; Striccoli, M.; Agostiano, A.; Curri, M. L. *J. Colloid Interface Sci.* **2008**, *325*, 558–566.
(46) Erogbogbo, F.; Yong, K.-T.; Roy, I.; Xu, G.; Prasad, P. N.; Swihart, M. T. *ACS Nano* **2008**, *2*, 873–878.
(47) Weissleder, R.; Bogdanov, A.; Neuwelt, E. A.; Papisov, M. *Adv. Drug Deliver. Rev.* **1995**, *16*, 321–334.
(48) Morales, M. P.; Bomati-Miguel, O.; Pérez de Alejo, R.; Ruiz-Cabello, J.; Veintemillas-Verdaguer, S.; O'Grady, K. *J. Magn. Magn. Mater.* **2003**, *266*, 102–109.
(49) Schmitz, S. A.; Taupitz, M.; Wagner, S.; Wolf, K.-J.; Beyersdorff, D.; Hamm, B. *J. Magn. Reson. Imaging* **2001**, *14*, 355–361.
(50) Cahill, K. S.; Gaidosh, G.; Huard, J.; Silver, X.; Byrne, B. J.; Walter, G. A. *Transplantation* **2004**, *78*, 1626–1633.
(51) de Vries, I. J. M.; Lesterhuis, W. J.; Barentsz, J. O.; Verdijk, P.; van Krieken, J. H.; Boerman, O. C.; Oyen, W. J. G.; Bonenkamp, J. J.; Boezeman, J. B.; Adema, G. J.; Bulte, J. W. M.; Scheenen, T. W. J.; Punt, C. J. A.; Heerschap, A.; Figdor, C. G. *Nat. Biotechnol.* **2005**, *23*, 1407–1413.
(52) A. Corr, S.; O'Byrne, A.; Gun'ko, Y. K.; Ghosh, S.; Brougham, D. F.; Mitchell, S.; Volkov, Y.; Prina-Mello, A. *Chem. Commun.* **2006**, 4474–4476.

Transmission electron microscopy (TEM) was performed on an FEI Tecnai 20 at 200 kV for high resolution imaging. Samples were drop cast and dried on carbon film copper grids. Energy dispersive X-ray (EDX) analysis was performed by scanning transmission electron microscopy (STEM) on the same microscope. Absorption spectroscopy was performed on a Perkin-Elmer Lambda 800 UV/vis spectrometer, and emission spectra were collected on a Perkin-Elmer LS50B emission spectrometer. Quantum yields were measured by comparison with fluorescence standards. Atto 390 (PPE and PFPV), fluoroscein (F8BT), and rhodamine 6G (MEH-PPV) were used. Electron spin resonance (ESR) measurements were performed on a Bruker EMX spectrometer. Samples were placed in glass ESR tubes prior to analysis. The samples were stored at room temperature. Magnetometric studies of the sample were performed in a Quantum Design magnetic property measurement system (MPMS-7).

MR images were acquired from samples of the MEH-PPV MF-SPNs in test tubes, and a range of concentrations were obtained through 2-fold serial dilution with water down from 0.0675 mg/mL iron oxide in the original sample. A sample of MEH-PPV SPNs was also prepared without iron oxide to serve as a control. The commercially available superparamagnetic iron oxide contrast agent Endorem (Guerbet GmbH, Germany) was also put into a test tube at a concentration based on the iron content of the original MEH-PPV BF-SPN sample, 0.0675 mg/mL. All the test tubes were placed in a 140 mm crystallizing dish filled with distilled water to form a phantom. MRI of the phantom was conducted using a transmit/receive quadrature head-coil on a 3.0 T scanner (Achieva, Philips Healthcare, Best, Netherlands). MR images were acquired from the transverse orientation to allow visibility of any sedimentation within the test tubes. A multigradient-echo sequence was utilized to produce a weighting in the images based on the transverse T_2^* relaxation time. The acquisition at multiple echo times (TEs) also allowed a parameter map of the R_2^* ($=1/T_2^*$) relaxation rate to be produced. This was based on a pixel-by-pixel fit of the signal decay in the MR images with TE to a monoexponential decay function, such that $S(\mathrm{TE}) = S_0 \cdot \exp(-R_2^* \cdot \mathrm{TE})$.

SHSY-5Y cells were maintained in Dulbecco's modified eagle's medium (DMEM) supplemented with 10% fetal bovine serum (FBS) 2 mM glutamine. Cells were seeded onto glass coverslips 24 h prior to experimentation. Cells were treated with a 1:10 dilution of MEH-PPV MF-SPNs in 500 μL of Optimem containing 10% FBS, 2 mM glutamine, and antimicrobials for 18 h. Cells were washed twice in phosphate buffered saline (PBS) and fixed in 3.7% paraformalde in PBS. Cells were permeabilized with 0.4% triton in PBS supplemented with 1% sucrose. The cells were then incubated with Alexa Fluor phalloidin (Invitrogen) and mounted using Vectasheild mounting medium containing 4′,6-diamidino-2-phenylindole. Visualization was carried out using a Leica DMIRE2 confocal microscope equipped with an LED diode laser to excite DAPI at 405 nm. The emission wavelength range chosen was 419−470 nm. The Alexa Fluor 488 conjugate and the nanoparticles were excited using an argon laser at 488 nm (and an emission range of 515−550 nm and 654−810 nm respectively). Visualization was carried out on the inverted samples, using a Leica HCX PL APO 63× oil immersion lens with a numerical aperture of 1.4 and a pinhole size equivalent to 1 Airy band resolution. An overlay was created using the Image J software package (http://rsbweb.nih.gov/ij/).

Results and Discussion

Mechanism of Formation. The basic premise for the formation of the MF-SPNs is the encapsulation of hydrophobic materials into micellar structures using amphiphilic molecules. The conjugated polymer and the oleic acid capped SPIONs are hydrophobic. The SPIONs, conjugated polymer, and phospholipids are all dissolved in DCM, and this solution is simply added to water and stirred. Rapid stirring induces the formation of DCM droplets throughout the aqueous solution, and as the phospholipids are amphiphilic it is expected that they orientate themselves such that their hydrophobic groups stay in the DCM phase, and their hydrophilic parts move into the water. This process then initiates the construction of a micelle type structure which encapsulates the conjugated polymer and SPIONs. As the DCM evaporates from the solution, the material inside the droplets is then compressed into hard spheres, forming a dispersion of MF-SPNs in water.

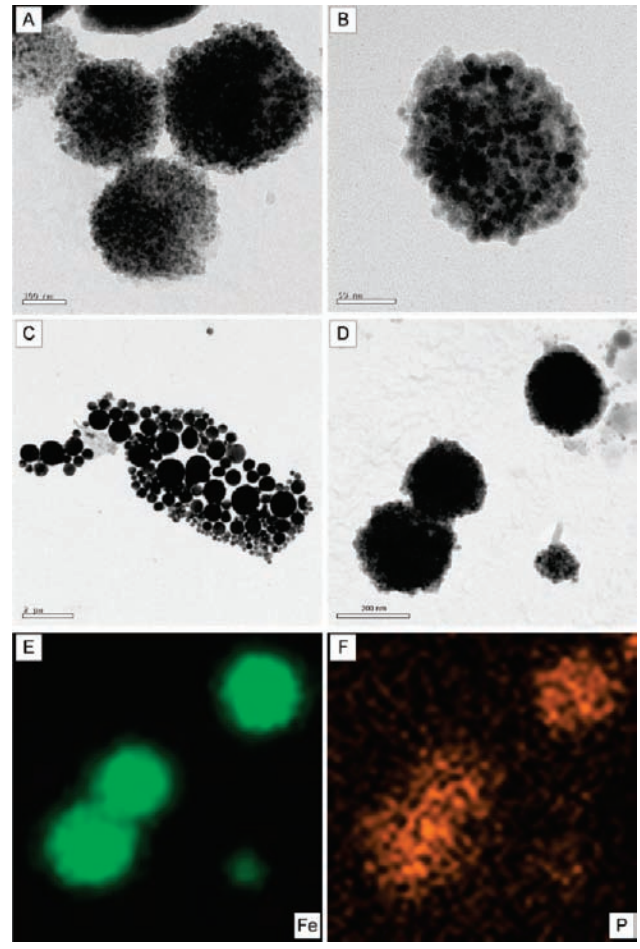

Figure 1. TEM images of the MF-SPNs. (A and B) TEM images of the MF-SPNs, PPE and PF respectively, in the size range of 100 to 400 nm. Scale bars are 100 and 50 nm respectively. (C) A distribution of PF MF-SPNs, exhibiting consistently spherical morphologies and a large size distribution. Scale bar represents 2 μm. (D) MEH-PPV MF-SPNs; scale bar represents 200 nm. (E and F) EDX elemental maps of the particles in image (D), indicating the presence of Fe and P, which supports the assertion that the MF-SPNs contain iron oxide and are capped by the phospholipids.

Four conjugated polymers were used in this work, chosen according to their wavelength of emission, to allow fluorescence across the visible spectrum.

Particle Analysis. The nature of this synthesis is that the amount of SPIONs encapsulated in the MF-SPNs is variable. To remove nonmagnetic material from the distribution, a magnet is used to separate off the magnetically responsive micelles, and the solid was washed with water several times. This process will be referred to as magnetic filtration hereafter. Figure 1 shows four TEM images of the MF-SPNs after this filtration process. Images A and B show PPE and PF micelles respectively. These particles, which are in the size range of 100 to 400 nm, are seen to be densely packed with the SPIONs. Figure

Table 1. MF-SPN Diameters Measured before and after Centrifugation

	PPE	PFPV	F8BT	MEH-PPV
Diameter before centrifugation (mean ± standard deviation)	589.5 ± 383.6	679.4 ± 384.8	359.2 ± 245.5	689.9 ± 486.0
Diameter after centrifugation (mean ± standard deviation)	157.7 ± 58.6	364.6 ± 169.9	209.8 ± 71.9	376.8 ± 265.8

1C shows distribution of PF MF-SPNs. It is seen that all of the particles are spherical, with a large distribution of sizes ranging from *ca.* 20 to 1000 nm. While it is generally preferred that particles are as small as possible, the successful use of larger particles has been demonstrated previously.[31]

Energy dispersive X-ray (EDX) spectroscopy was performed on the samples by scanning transmission electron microscopy (STEM) imaging to produce elemental maps of the MF-SPNs. Figure 1D shows three MEH-PPV MF-SPNs, *ca.* 200 nm in diameter. Images E and F are elemental maps, with iron shown in green and phosphorus shown in orange. These maps show a strong correlation of these elements with the nanoparticles, indicating the presence of phosphorus from the phospholipid molecules and iron from the iron oxide. These data provide important confirmation that the MF-SPNs are encapsulated in the phospholipids and contain iron oxide, as expected.

The mean particle diameters of the MF-SPNs were measured from the TEM images and ranged from 350 to 700 nm for the four different polymer varieties. The size distributions were broad and included particles well above 1 μm in their range. In an attempt to remove the largest particles from the distributions, the magnetically filtered solutions were then centrifuged. After centrifugation, the sediment was discarded and the solution was further analyzed. There was a consistent drop in the MF-SPN diameter, with the MF-SPNs now ranging from *ca.* 160 to 380 nm. The smallest particles obtained were the PPE MF-SPNs, at 157.7 ± 58.6 nm. The full results are shown in Table 1, and Figure 2 shows the TEM images of the MF-SPNs after centrifugation.

ESR spectroscopy was used to study the magnetic properties of MEH-PPV MF-SPNs over a period of 6 months (Supporting Information, Figure 1). These results were compared with those of SPIONs in water alone. There was no significant change in magnetic properties observed in the MEH-PPV MF-SPNs over the 6 months, whereas the SPIONs in water showed definite signs of degradation in magnetic integrity. This suggests that the SPIONs are chemically stable within the MF-SPNs.

Magnetometric studies of the MF-SPNs below (10 K) and above (300 K) the blocking temperature of SPIONS confirmed that they particles are indeed superparamagnetic (Supporting Information, Figure 2). A negligible hysteresis is present at 300 K due to the irreversibility of the superconducting magnet in SQUID measurements.

Optical Characterization. The absorption and emission spectra were recorded for the MF-SPN solutions before and after magnetic filtration and centrifugation. It was found that the absorption spectra are dominated by light absorption of the SPIONs. Figure 3A shows the absorption spectra of the MF-SPN reaction solutions, with the absorption spectrum of the SPIONs shown in black. From 800 to 600 nm, the absorption is completely due to the SPIONs, with all spectra following the same line. Below 600 nm, the absorption of the conjugated polymers becomes evident. The absorbance of all samples increases with decreasing wavelength, which is due to absorption by the phospholipids and SPIONs below 400 nm, with F8BT showing particularly high absorbance because it absorbs strongly in this region anyway. Figure 3C shows the absorption spectra of the MF-SPNs after magnetic filtration and centrifugation, with the SPIONs again shown in black. The absorption of the SPIONs is even more dominant in these spectra. The process of magnetic filtration has the effect of removing any pure SPN micelles (those without any SPION content) and any excess phospholipid from the solutions, thus reducing the characteristics of these in the spectra.

Figure 3B shows the emission spectra of the MF-SPN reaction solutions. It is seen here that the emission from the four separate polymers covers the visible range, from blue to red. When conjugated polymers are confined in a solid, they exhibit marked changes in their optical characteristics compared to when they are free in dilute solutions. In solution, the polymer chains do not interact strongly with one another, so the optical behavior is characteristic of the individual chains. As conjugated polymers are semiconductors, photoluminescence occurs by exciton formation and recombination. The absorption and emission of an individual polymer chain are satisfactorily explained by the *intra*chain exciton. However, the behavior of bulk polymer systems is largely governed by the *inter*chain interactions that arise because of the close proximity of neighboring chains.[25] The emission spectra of the MF-SPNs exhibit the usual vibronic shoulders expected from fluorescence emission. However, there are some additional features in the emission spectra which arise because of interchain interactions of the conjugated polymer chains in the MF-SPNs. For PPE, the emission spectrum shows high intensity peaks at lower energies relative to the primary peak, which are not present in the emission of PPE in solution (DCM). With reference to reports on PPE polymers in thin films, we suggest that these peaks are caused by the formation of emissive excimers.[53]

Aggregation of conjugated polymers in the solid state gives rise to electron delocalization across adjacent chains.[25] These aggregated regions exhibit lower absorption and emission energies and are particularly prevalent in solid state conjugated polymer systems. The emission of MEH-PPV in the solid state comes completely from these low energy regions, which is observed in the MEH-PPV MF-SPNs as it red-shifts by 34 nm compared to MEH-PPV in DCM.[54] The PFPV MF-SPNs exhibit a much smaller shift in emission (5 nm), suggesting aggregation is not as dominant for this polymer in the solid state. The F8BT MF-SPNs exhibit particularly interesting optical behavior, with a high intensity lower energy peak. This polymer is known to exhibit bimodal emission, from aggregated and nonaggregated sites, and it would appear that the emission from low energy sites is favored in the presence of the SPIONs.[55] This may be due to more efficient energy funneling to the lower energy state or because of energy transfer from the SPIONs to aggregate sites. Figure 3D shows the emission spectra of the MF-SPN solutions after magnetic filtration and centrifugation. The most

(53) Bunz, U. H. F.; Imhof, J. M.; Bly, R. K.; Bangcuyo, C. G.; Rozanski, L.; Vanden Bout, D. A. *Macromolecules* **2005**, *38*, 5892–5896.
(54) Grey, J. K.; Kim, D. Y.; Norris, B. C.; Miller, W. L.; Barbara, P. F. *J. Phys. Chem. B* **2006**, *110*, 25568–25572.
(55) Grey, J. K.; Kim, D. Y.; Donley, C. L.; Miller, W. L.; Kim, J. S.; Silva, C.; Friend, R. H.; Barbara, P. F. *J. Phys. Chem. B* **2006**, *110*, 18898–18903.

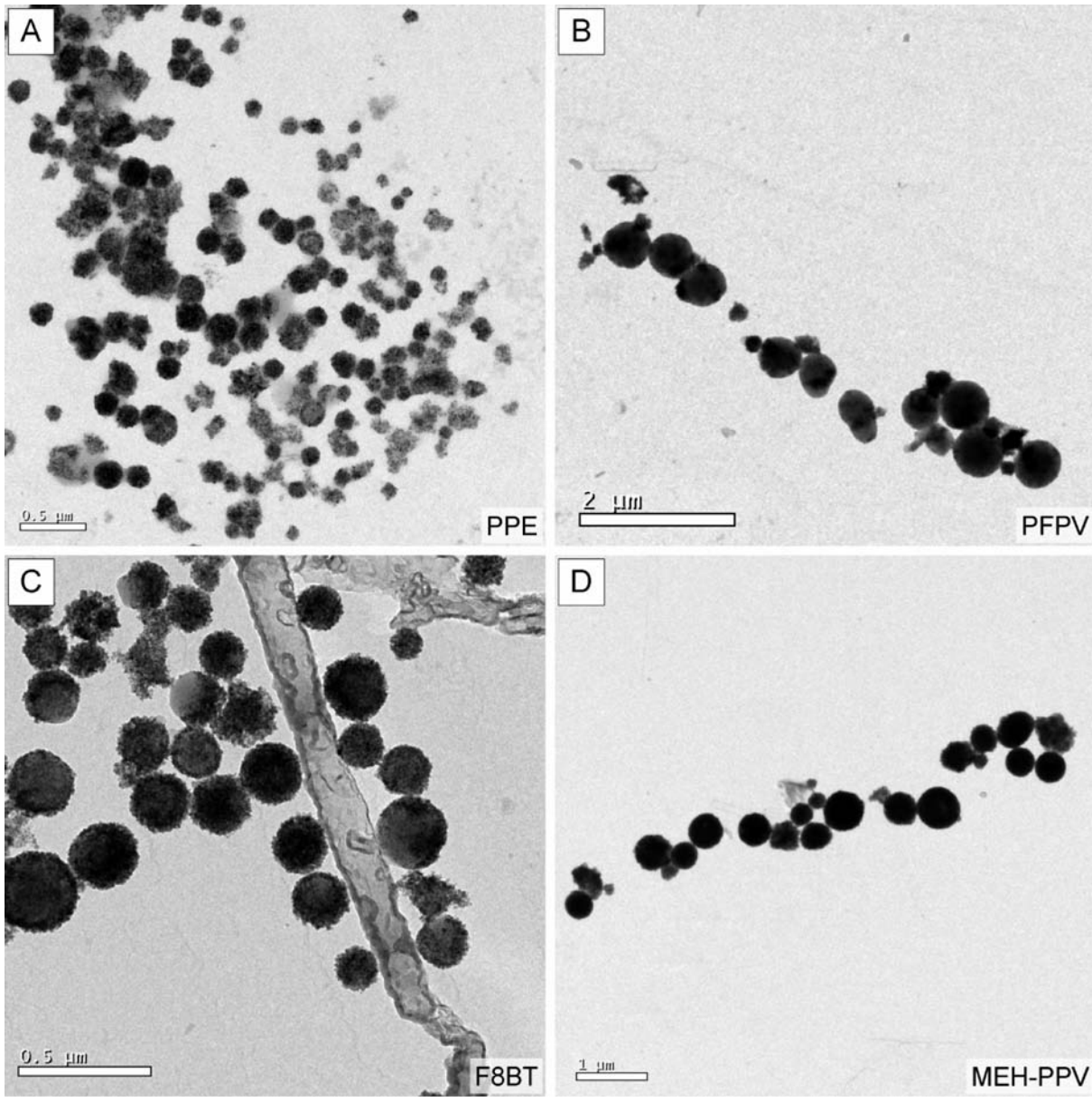

Figure 2. TEM images of the MF-SPNs of (A) PPE, (B) PFPV, (C) F8BT, and (D) MEH-PPV with scale bars of 0.5, 2, 0.5, and 1 μm respectively. The constituent polymers are also shown in the inlays. The MF-SPNs exhibited a consistent decrease in diameter after the aqueous solutions were centrifuged to remove the largest particles.

obvious difference is the increased intensity of the secondary peak in F8BT relative to the higher energy peak. As the filtration process removes any micelles without SPIONs, this presents strong evidence that the lower energy shoulder is arising due to the presence of the SPIONs in the system.

Conjugated polymers exhibit high fluorescence quantum yields in solution (e.g., MEH-PPV is 30% in chlorobenzene[56]) due to efficient absorption and emission of energy by isolated polymer chains. However, in the solid state they exhibit reduced quantum yields. It is thought that excited state excitons can decay nonradiatively to the ground state in a number of ways in solid state conjugated polymers, for example at defect sites.[25] Additionally, interchain species generally exhibit weaker emission compared to the intrachain species, and they have longer radiative lifetimes due to a poor energetic overlap of the interchain excited states with the single chain ground state.[25] The fluorescence quantum yields for the PPE, PFPV, F8BT, and MEH-PPV MF-SPNs were 1%, 1.2%, 2.2%, and 0.4% respectively. An additional reason for the drop in quantum yield is the strong absorption by the SPIONs, which likely does not contribute to the emission from the conjugated polymers. This means a proportion of the absorbed energy is lost as heat. Additionally, fluorescence quenching by the SPIONs may contribute to the low quantum yield, which has been observed in conjugated polymer composites with fluorescent dyes[36] and quantum dots,[57] and is typically a problem with fluorescent-magnetic nanocomposites.[12] The quantum yield remained relatively stable before and after removal of the largest particles by centrifugation, suggesting it is not dependent on particle size within the range covered here. Although the quantum yields

(56) Amautov, S. A.; Nechvolodova, E. M.; Bakulin, A. A.; Elizarov, S. G.; Khodarev, A.; Martyanov, D. S.; Paraschuk, D. Y. *Synth. Met.* **2004**, *147*, 287–291.

(57) Hong, S.-K. *Physica E* **2005**, *28*, 66–75.

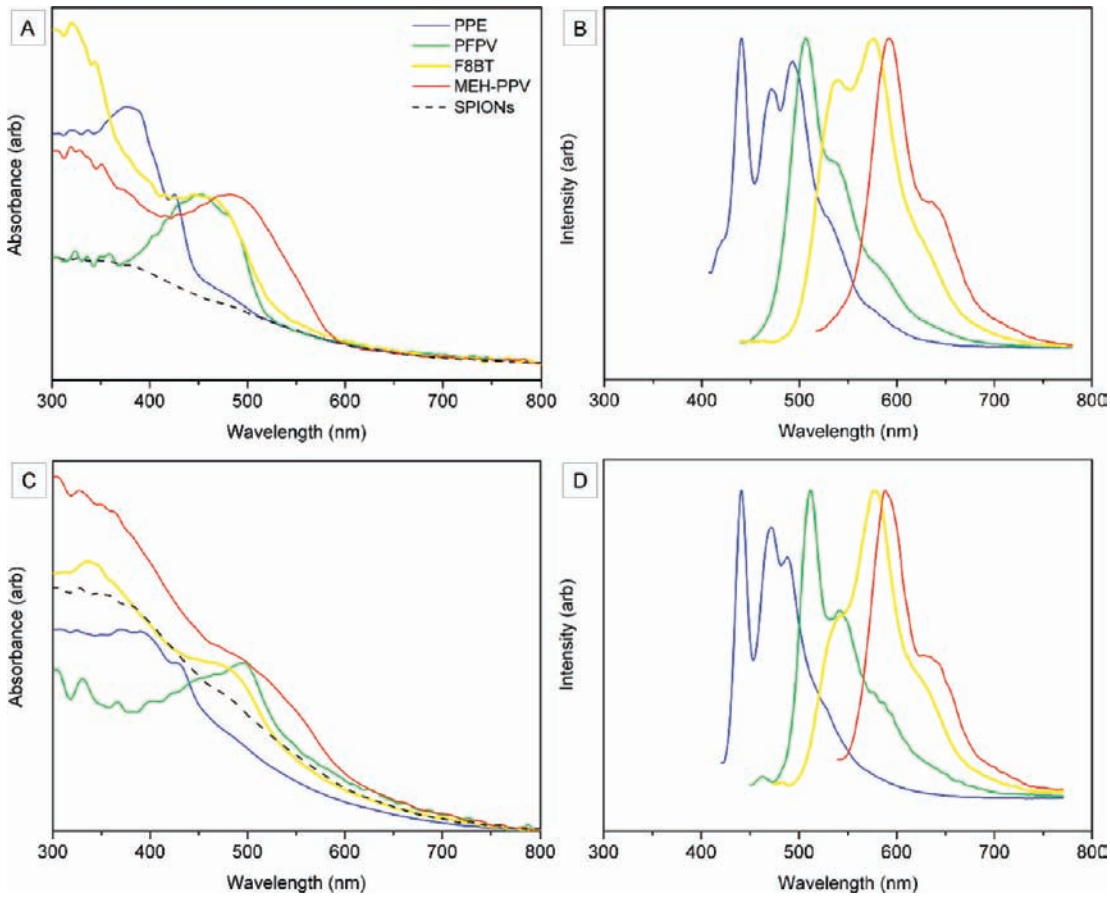

Figure 3. Absorption (left) and emission (right) spectra of the MF-SPNs in aqueous solutions: (A and B) prior to magnetic filtration and centrifugation; (C and D) after magnetic filtration and centrifugation. The MF-SPNs were all excited at 400 nm, except MEH-PPV which was excited at 500 nm. The dashed black line represents the absorption of the SPIONs, which was reasonably dominant in the absorption spectra.

measured here are relatively low, as conjugated polymers exhibit large extinction coefficients (meaning they absorb light strongly), the fluorescence brightness remains high enough for fluorescence imaging applications. The photostability of conjugated polymers in cell imaging has been investigated previously and found to be excellent.[32]

Figure 4 shows the aqueous MF-SPN solutions after magnetic filtration and centrifugation. Image A shows the four solutions, corresponding to each conjugated polymer, in cuvettes. When exposed to 365 nm UV light, these solutions were seen to fluoresce brightly, as seen in image B. The solutions were then exposed to a magnetic field, and the MF-SPNs collected at the side of the cuvette, leaving an optically clear solution behind (image C). Upon exposure to UV (image D), the material at the side of the cuvette was seen to maintain its fluorescence, indicating that the MF-SPNs were indeed magnetically responsive and fluorescent, simultaneously.

Preliminary Studies in Biological Imaging. Many of the applications envisaged for multifunctional nanoparticles have been in biological sciences. To demonstrate the potential of the MF-SPNs developed in this work for use in such applications, two preliminary studies were performed. First, MRI was performed on the aqueous MF-SPN samples to study their MR properties relative to a standard iron oxide based contrast agent (Endorem). Second, the MF-SPNs were imaged in fixed cells to assess their potential as fluorescent markers and to look for signs of cell toxicity. The reaction solutions were studied without magnetic filtration or centrifugation.

In the MRI studies, MEH-PPV MF-SPNs were shown to have a shortening effect on the transverse T_2^* relaxation time. This was visible from the signal loss in the test tubes of the MF-SPNs (and the Endorem) compared to the background of water in the phantom, as shown in Figure 5A. The images from multiple TEs (echo times) were used to fit the signal at each pixel to the exponential decay function and produce a parameter map of the R_2^* ($=1/T_2^*$) relaxation rate (Figure 5B). This provided a quantitative measurement of the effect that the MF-SPNs had on the transverse magnetization in MR. The 2-fold serial dilution allowed a chart of relaxation rate vs concentration to be produced (Figure 5C). This showed a linear relationship and indicated a detection limit might be quantifiable based on iron oxide concentration. The MF-SPNs were compared with pure polymer SPNs (without iron oxide). Interestingly, the sample containing SPNs without iron oxide produced R_2^* values comparable to those for the MF-SPN sample at the lowest concentration of iron oxide. This might suggest that a relatively small amount of iron is required in the MEH-PPV SPNs to induce a distinguishable MR effect. The amount of SPIONs encapsulated varied between the polymer micelles. As such there was an increased variation in R_2^* values recorded from those polymer samples with greater concentrations. This is also evident from the relatively homogeneous color of the R_2^* map from the Endorem compared to the polymer samples. The R_2^* values measured from the Endorem sample and the original MEH-PPV MF-SPN sample, with the same iron content, were (134 ± 40)

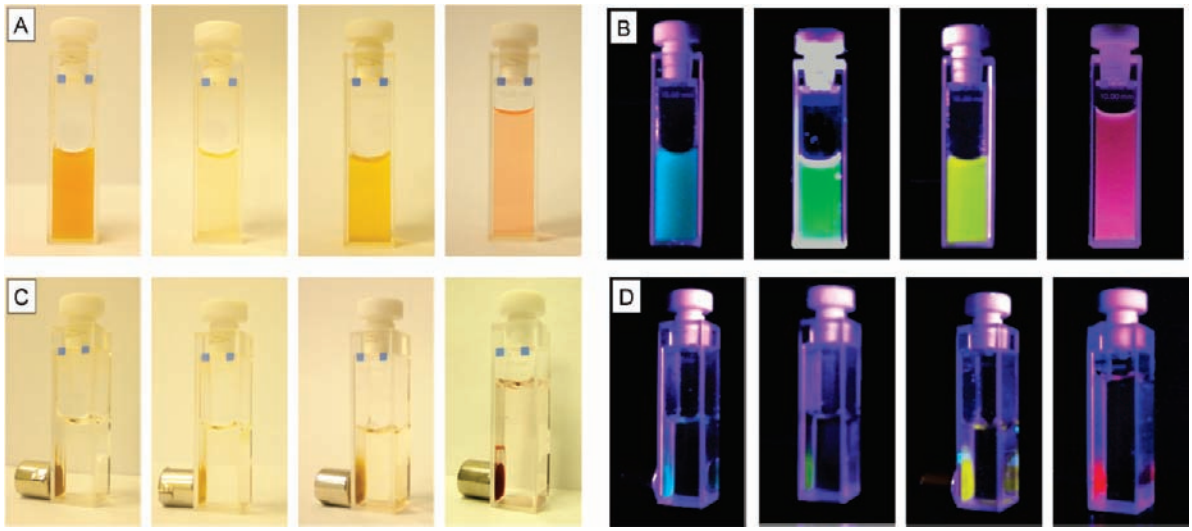

Figure 4. Aqueous MF-SPN solutions under UV illumination and magnetic fields. (A) The four aqueous MF-SPN solutions, PPE, PFPV, F8BT, and MEH-PPV from left to right. (B) The same solutions under 365 nm UV light, where they are seen to fluoresce brightly. (C) When exposed to a magnetic field, the MF-SPNs respond and collect at the side of the cuvette. (D) The MF-SPNs remain fluorescent under UV while in the magnetic field.

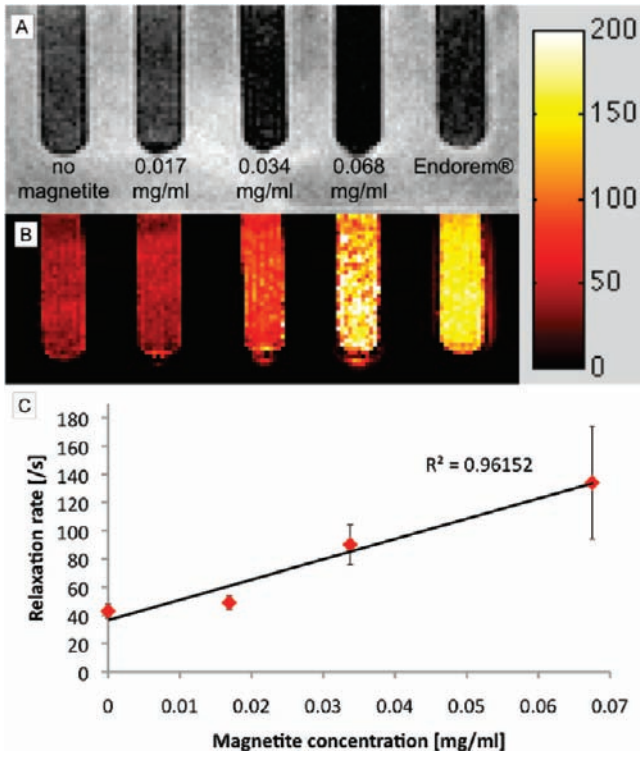

Figure 5. (A) shows a T_2^*-weighted negative contrast image acquired at TE = 14 ms with the four BF-SPN samples on the left and the Endorem sample positioned on the right. The Endorem sample was prepared with an iron content to match the original MEH-PPV SPN sample. (B) is a R_2^* parameter map calculated from an exponential fit of the signal decay from each pixel with TE. The color-bar to the right indicates the R_2^* relaxation rate in the map with units of [s^{-1}]. (C) shows the R_2^* measured from the parameter map for each polymer sample and plot against the corresponding concentration of iron oxide (magnetite) with a line of best fit from linear regression.

and (152 ± 10) s^{-1} respectively. However, for a more meaningful comparison, and to further assess the efficacy of the MF-SPNs as an MR contrast agent, a more homogeneous SPION distribution is required. The results from the T_2^*-weighted images though did suggest that the MF-SPNs had an MR effect and dephased the signal, with the effect linearly increasing with the iron oxide concentration in the solutions.

In the cell imaging studies, SH-SY5Y neuroblastoma cells were treated with MEH-PPV MF-SPNs for 18 h for imaging and assessment of toxicity over a 48 h period. These time points represent exposure relevant for cell culture experimental paradigms. The distributions of nanoparticles in cross sections throughout the depth of the cell were determined to assess whether the MF-SPNs were taken up by the cells or whether they were just attached to the surface. The nucleus and actin were stained to indicate the cytoplasm and cell periphery, and cross sections from the top, middle, and bottom of cell were imaged (Figure 6A, B, and C respectively). In the middle sections of the cell, characteristic clustering of MF-SPNs is observed, unilaterally within the perinuclear zone. This clustering suggests that the nanoparticles are contained within vesicles, as one would expect a uniform distribution throughout the cell if the particles were in the cytoplasm. The size distribution of the MF-SPNs is large, and a size dependency was observed for cellular uptake. In the images in Figure 6, and particularly in C, some larger MF-SPNs are present which appear to be sitting between the cells. These particles, which are in the region of 1 μm, are consistent with the larger particles observed in Figure 1. The MF-SPNs which were taken up by the cells, and observed to be clustered near the nucleus, are the much smaller ones. The SPION content of the particles which were taken up is unknown; however it is expected that some of the smaller MF-SPNs, as observed in Figure 2, could be taken up. Although the SPION content of the different micelles present in the image is unclear, it seen that sufficient fluorescence brightness for imaging applications is maintained.

Control (nontreated) cells were compared to treated cells from two independent preparations of MEH-PPV MF-SPNs to assess cell viability. Figure 6D shows the growth curve of the MF-SPN stained cells against an unstained control cell population. Over the 48 h period of measurement there was no change in growth rate between the control cells and treated cells, demonstrating that the MF-SPNs do not affect growth of the

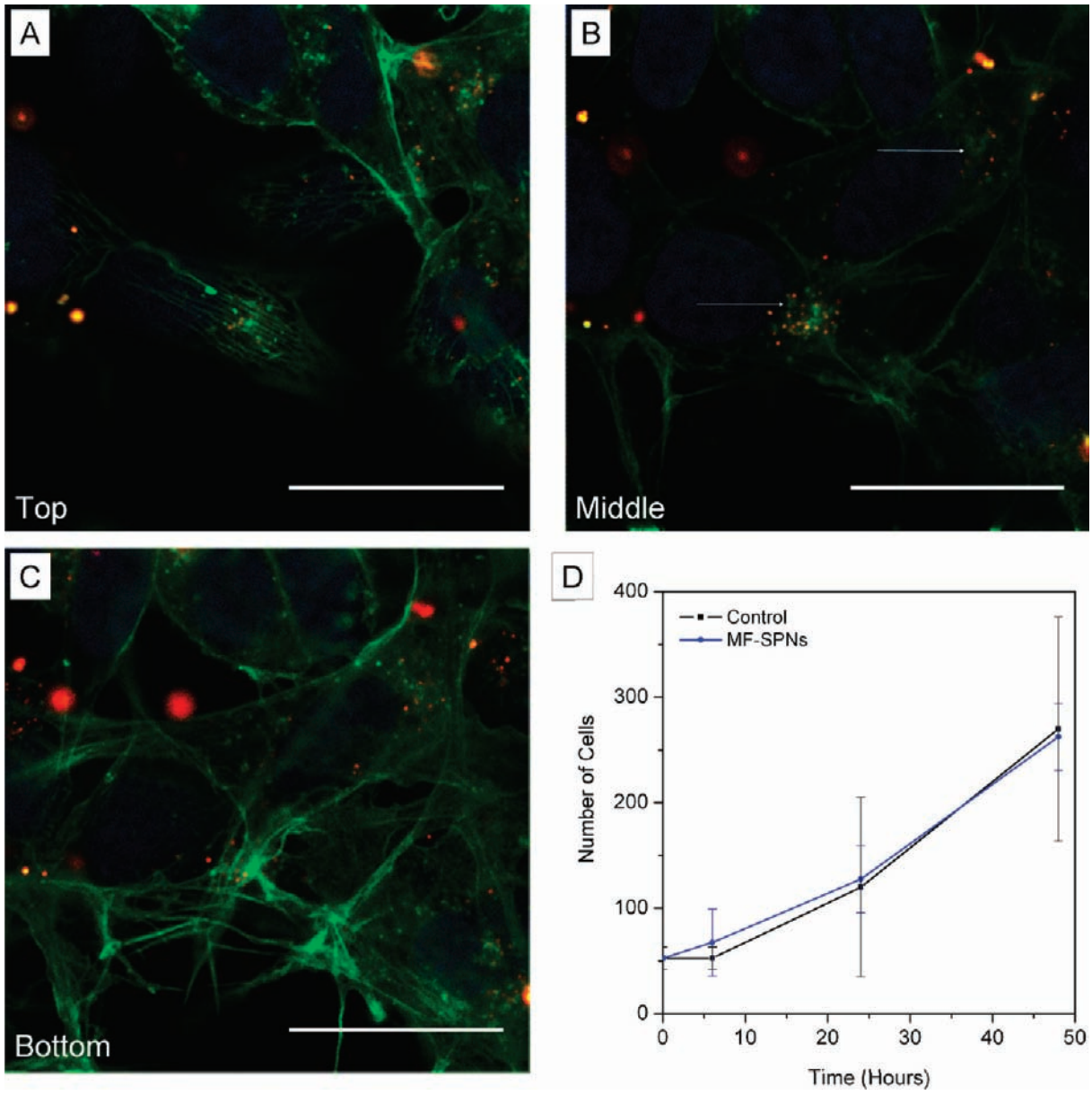

Figure 6. Confocal images of SH-SY5Y treated with MF-SPNs. Cells were treated for 18 h with MEH-PPV MF-SPNs. Sections were imaged from the (A) top, (B) middle, and (C) bottom of cells (at +3.7, 0, and −2.0 μm respectively). Fluorescent staining shows MF-SPNs (red), nuclei (blue), and actin (green). The arrows indicate the clustered distribution of MF-SPNs in the middle section of the cell. The scale bars represent 25 μm. (D) A growth curve of the MF-SPN stained cells and an unstained control cell population. Over 48 h it was observed that the MF-SPNs did not adversely affect growth of the cells, suggesting they are nontoxic.

cells. Further observation showed no change in cell or nuclear morphology over this period. This demonstrated that the MF-SPNs were not toxic to the cells. Furthermore, even though the MEH-PPV MF-SPNs were seen to have a low quantum yield, they still performed well as fluorescent markers due to their large extinction coefficients. These results suggested that the nanoparticles used in this study would be suitable for fluorescent imaging applications.

Conclusions

In this work we have demonstrated a simple and robust method for the synthesis of multicolored bright fluorescent-magnetic nanoparticles by the encapsulation of hydrophobic conjugated polymers and iron oxide nanoparticles in phospholipid micelles. These MF-SPNs responded to an external magnetic field and maintained strong fluorescence. Superparamagnetic properties of the SPIONS were confirmed by MPMS studies, their morphology and elemental composition were confirmed by TEM and EDX analyses, and magnetic stability was confirmed by ESR studies. They were shown to provide contrast enhancement in MRI due to their affect on the transverse T_2^* relaxation times. Finally, they were successfully imaged inside cells where they acted as bright, stable, and nontoxic fluorophores. There is great potential for development of these nanostructures. For example, targeting functionality should be readily achieved by the use of functionalized phospholipids which provide a ready means of conjugation with other structures, such as biomolecules. Fine tuning of the micellar structure should allow further control of size and size distribution. The nature of the

synthesis should allow the incorporation of other MRI active nanoparticles, gadolinium for instance.[58] Finally, with the variety of conjugated polymers which are commercially available, it is easy to envisage fine-tuning of the optical properties of this system for specific applications.

(58) Vuu, K.; Xie, J. W.; McDonald, M. A.; Bernardo, M.; Hunter, F.; Zhang, Y. T.; Li, K.; Bednarski, M.; Guccione, S. *Bioconjugate Chem.* **2005**, *16*, 995–999.

Acknowledgment. We acknowledge KCL for a studentship (P.H.) and KCL Business for funding (M.G., P.H.).

Supporting Information Available: ESR plots comparing the behavior of SPIONs in water to SPIONs in the MF-SPNs over a period of 6 months and hysteresis curves of the iron oxide at 300 K and 10 K. This material is available free of charge via the Internet at http://pubs.acs.org.

JA1031634